Velocity Map Imaging Study of the O_2 Ion-Pair Production at 17.499 eV: Simultaneous Parallel and Perpendicular Transitions

Yusong Hao, Chang Zhou, and Yuxiang Mo*

Department of Physics and Key Laboratory for Atomic and Molecular Nanosciences, Tsinghua University, Beijing 100084, China

Received: April 14, 2005; In Final Form: May 13, 2005

The fine structure resolved photofragment $O^-(^2P_j)$ image from the O_2 ion-pair production at 17.499 eV has been recorded. The branching ratio for producing the low energy spin−orbit $O^-(^2P_{3/2})$ component to the high energy spin−orbit $O^-(^2P_{1/2})$ component is 1:0.78 and the optical transitions for them correspond to perpendicular and parallel transitions, respectively. The anisotropy parameters, 1.64 for channel producing $O^-(^2P_{1/2})$ and −0.35 for $O^-(^2P_{3/2})$, suggest that the dissociation proceeds via the states with symmetry $^3\Sigma_u^-$ and $^3\Pi_u$, respectively. Although the main mechanisms for the O_2 ion-pair production are the predissociation via the intermediate Rydberg states, the direct dissociation mechanism for the channel producing $O^-(^2P_{1/2})$ may also be involved.

Introduction

Photoexciation of molecules above the ionization potential will not only lead to the direct ionization of molecules but also to other phenomena via the decay of the so-called molecular superexcited states, such as autoionization, dissociative ionization, neutral dissociation, and ion-pair production.[1] The ion-pair production which occupies only a small proportion in the overall decay process cross-sections has been given much attention.[1] Because the minimum energy position in the potential curve for ion-pair is usually far away from the equilibrium structure of the neutral molecular state, the cross sections for direct excitation from the neutral molecular states to the ion-pair states are small due to the poor Franck−Condon factors. Therefore, the production of ion-pair states is often explained as the predissociation of the molecular Rydberg states. Among a few ion-pair productions studied, the ion-pair production of O_2 has attracted more attention.[2−5] The high-resolution photofragment yield spectra for O^- from the O_2 ion-pair production showed some sharp resonances, and this was in terms of the predissociation of molecular Rydberg states.[2,3] As it is well-known in the molecular photodissociation of neutral fragments,[6−7] the angular distribution of fragments can provide direct evidence about the dissociation dynamics and it is specially true for the photodissociation of diatomic molecules. The predissociation mechanism of O_2 ion-pair production and the resonance peaks observed in the photofragment yield spectra would result in a lower anisotropic angular distribution of the O^- fragments than that from the direct dissociation. For a nonzero anisotropy parameter β, it will also suggest the optical transition properties.

In another respect, the ion-pair production of O_2 may produce the fine structure components of O^- atoms, i.e., O^- ($^2P_{3/2}$) and O^- ($^2P_{1/2}$). The branching ratio for the two components and the fine structure resolved photofragment angular distributions would provide insights about the ion-pair production dynamics. Recently, the velocity map imaging method[8] has been applied to study the ion-pair production of CH_3Cl, CH_3F, and F_2.[9−11] In this work, we report such a study on the O_2 ion-pair production at 141 139.3 cm^{-1} (17.499 eV) by recording the O^- velocity map image

$$O_2(X^3\Sigma_g^-) + 141\ 139.3\ cm^{-1} \rightarrow O^-(^2P_{3/2}) + O^+(^4S_{3/2}) + 1818.1\ cm^{-1} \quad (1a)$$

$$\rightarrow O^-(^2P_{1/2}) + O^+(^4S_{3/2}) + 1641.0\ cm^{-1} \quad (1b)$$

Experimental Section

The experimental machine used in this study has been described in detail previously.[11,12] Briefly, the coherent XUV radiation ($3\omega_1$) was generated by using the resonance enhanced frequency tripling of a focused laser beam in a pulsed Kr jet. The fundamental laser beam (ω_1) was prepared by tripling of a dye laser which was pumped by a Nd:YAG (20 Hz) laser. The $2\omega_1$ (94 092.9 cm^{-1}) was fixed at the Kr transition of $4p^5(^2P_{3/2})5p[1/2]_0 \leftarrow (4p^6)^1S_0$. The apparatus consists of four vacuum chambers, namely, (a) the frequency mixing chamber, which houses the pulse Kr jet (ø1 mm); (b) the monochromonator chamber, which is equipped a gold coated toroidal grating; (c) the beam source chamber, which houses a pulse valve (ø0.7 mm) to produce a pulse molecular beam; the beam enters into the ionization chamber through a skimmer (ø1 mm); (d) the ionization chamber, which houses an electrostatic lens system for velocity map imaging[8] and a time-of-flight tube equipped with imaging quality dual MCP (ø50 mm and a channel pitch of 12 μm, North Night Vision, Nanjing Branch). The imaging plane is perpendicular to the molecular beam, and the distance from it to the XUV laser beam and molecular beam interaction point is 94 cm. The mass gate to select the O^- ion was a positive voltage pulse of 100 ns width and 1800 V high provided by a high voltage pulse generator (PVM-4140, DEI). The ion images were captured by a deep cooled CCD camera with a resolution of 1024 × 1024 $pixel^2$ (Andor DU-434). The pure oxygen gas (99.99%) was used in the experiments. The stagnation pressure of the sample was about 1000 Torr.

* To whom correspondence should be addressed. E-mail: ymo@mail.tsinghua.edu.cn.

10.1021/jp0519262 CCC: $30.25
Published on Web 06/11/2005

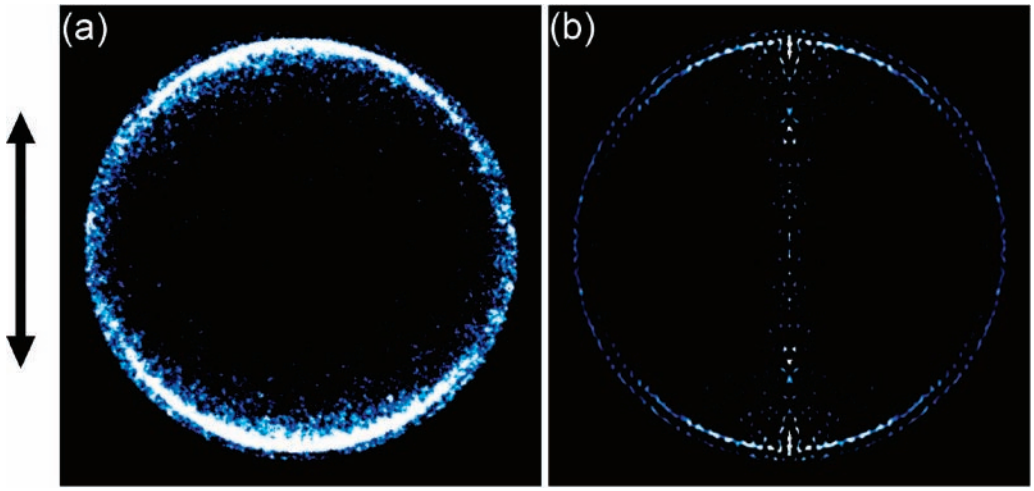

Figure 1. (a) Experimental raw image of O^- photofragment from the O_2 ion-pair production at 17.499 eV in the electric field of 300 V/cm. The polarization of the XUV laser is parallel to the image plane and is shown in the figure. (b) 2-D slice of the reconstructed 3-D sphere. The Wiener filter was used to deconvolute partially the instrumental factors. The outer ring corresponds to $O^-(^2P_{3/2})$ and the inner ring corresponds to $O^-(^2P_{1/2})$.

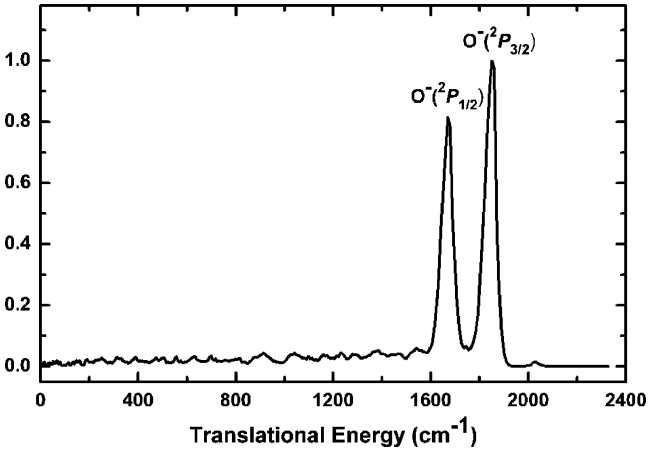

Figure 2. Center of mass translational energy distribution of photofragments for the O_2 ion-pair production at 17.499 eV in the electric field of 300 V/cm. The two peaks correspond to $O^-(^2P_{3/2})$ and $O^-(^2P_{1/2})$, respectively.

Results and Discussion

Figure 1a shows the experimental raw image of O^- from the O_2 ion-pair production at 141 139.3 cm^{-1} (17.4990 eV or 70.8520 nm) in the electric field of 300 V/cm. The polarization of the XUV radiation is parallel to the image plane and along the up and down direction. The Abel-Hankel transform[13] of Figure 1a showed clearly that two partially overlapped components exist. Many instrumental factors have decreased the resolution of the image, such as the space resolution of the dual MCP plates. To deconvolute part of the instrumental factors, we have applied the least-squares (Wiener) filter[14] to Figure 1a before the Abel-Hankel transform. To eliminate the so-called salt noises in the image, we also used the harmonic mean filter in the imaging processing.[14] Figure 1b shows the 2-D slice through the reconstructed 3-D sphere. Two circles are completely separated in Figure 1b. The outer circle corresponds to the formation of ground $O^-(^2P_{3/2})$, and the inner one corresponds to the excited $O^-(^2P_{1/2})$. Based on Figure 1b, the center of mass (CM) translational energy distribution for the O_2 ion-pair production can be obtained and is shown in Figure 2. The energy spacing between $O^-(^2P_{3/2})$ and $O^-(^2P_{3/2})$ is known accurately[15] and is used to calibrate the CM translational energy distribution. The fine structure branching ratio can be obtained by integrating the peak areas in Figure 2 and is listed in Table 1.

TABLE 1: Fine Structure Resolved Anisotropy Parameters and the Branching Ratio for the O_2 Ion Pair Production,[a]

$$O_2(X^3\Sigma_g^-) \xrightarrow{17.499\ \text{eV}} O^-(^2P_{1/2,3/2}) + O^+(^4S_{3/2})$$

channel	anisotropy parameter β	branching ratio
$O^-(^2P_{3/2}) + O^+(^4S_{3/2})$	−0.35(10)	1.0
$O^-(^2P_{1/2}) + O^+(^4S_{3/2})$	1.64 (10)	0.78(5)

[a] The numbers in parentheses are uncertainties in the last two or one digits of the data, which are estimated by data fitting and the imaging processing.

The angular distributions for $O^-(^2P_{3/2})$ and $O^-(^2P_{1/2})$ can be extracted from Figure 1b and they are shown in Figure 3, panels a and b, respectively. The anisotropy parameters β for the two spin−orbit components are listed in Table 1. They are obtained by using the following equation to fit the curves in panels a and b in Figure 3, respectively

$$f(\theta) \propto 1 + \beta P_2(\cos\theta) \quad (2)$$

where θ is the angle between the recoil velocity and the polarization direction of the XUV laser, and $P_2(x)$ is the second-order Legendre polynomial. In the limiting case of parallel or perpendicular transitions, β equals 2 or −1.

The threshold energy for ion-pair production (E_{tipp}) of O_2 at zero electric field has been determined accurately.[16] The E_{tipp} depends on the applied electric field.[11,16,17] However, for the electric field strengths of 300 and 500 V/cm which we have used, we found that the fine structure branching ratios are the same within our experimental uncertainties and also there are no appreciable differences in the anisotropy parameters β.

The ion-pair production of O_2 in the energy range 17.22−18.23 eV (or in the wavelength range 72−68 nm) has been assigned predominantly from the predissociation of two Rydberg series (strong and weak) which are converged to O_2^+ ($b^4\Sigma_g^-$).[2−5] The two Rydberg series which arise from the one photon absorption are

$$X^3\Sigma_g^- \rightarrow KK(\sigma_g2s)^2(\sigma_u2s)^2(\sigma_g2p)^1(\pi_u2p)^4(\pi_g2p)^2np\sigma_u,\ R^3\Sigma_u^- \quad (3a)$$

$$X^3\Sigma_g^- \rightarrow KK(\sigma_g2s)^2(\sigma_u2s)^2(\sigma_g2p)^1(\pi_u2p)^4(\pi_g2p)^2np\pi_u,\ R^3\Pi_u \quad (3b)$$

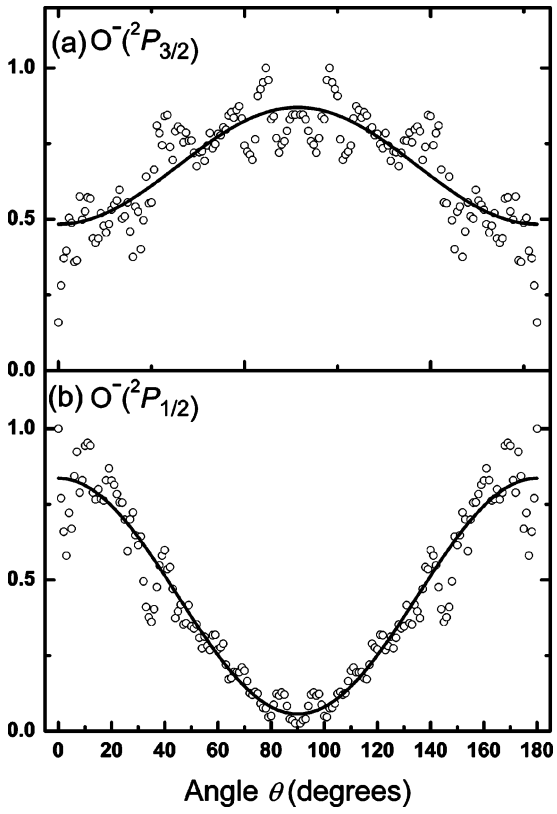

Figure 3. Angular distribution of O^- photofragments from the O_2 ion-pair production at 17.499 eV for (a) $O^-(^2P_{3/2})$, and (b) $O^-(^2P_{1/2})$. The small circles represent the experimental data and the lines are fits obtained using the anisotropy parameters β listed in Table 1.

where R represents the Rydberg state. If we use the united atom model instead of the above separated atom model for molecular orbitals, the above transitions correspond to excitations from $3s\sigma_g$ to Rydberg orbitals $np\sigma_u$ and $np\pi_u$. The first transitions (eq 3a) form the strong series, whereas the second (eq 3b) ones form the weak series. We note that eq 3a corresponds to a parallel transition and eq 3b corresponds to a perpendicular transition.

For the transition at 17.499 eV of O_2, the PFI-ZEKE (pulsed field ionization and zero electronic kinetic energy) signals have not been observed.[18] This means that long-lived high Rydberg states cannot be excited for this excitation energy. An examination of the previously measured two Rydberg series[19] converging to O_2^+ ($b^4\Sigma_g^-$) show also that its two nearest bands are associated with low Rydberg states only and they are (a) strong series at position 141 039 cm^{-1} with assignment (4,0) band, $n = 5$, and (b) weak series at position 141 147 cm^{-1} with assignment (0,0) band, $n = 6$. Considering the rotational excitation and the rotational constants of O_2^+ ($\sim$1 cm^{-1}), the XUV photon may excite the weak series resonantly; however, it is too far away from the band origin of the strong series and hence the resonant excitation could not occur for the strong series. Based on the above reason, we would expect that the O^- fragment from the O_2 ion-pair production at 17.499 eV has negative anisotropy parameter β, however, with absolute value much less than 1 due to the perpendicular transition and the predissociation mechanism. Surprisingly, the observed results as listed in Table 1 show that both parallel and perpendicular transitions appear, and furthermore, the parallel one correlates with the high energy spin−orbit component $O^-(^2P_{1/2})$, and the perpendicular one correlates the low energy spin−orbit component $O^-(^2P_{3/2})$, i.e.

$$O_2(X^3\Sigma_g^-) + 141139.3\ cm^{-1} \rightarrow O_2(R^3\Pi_u) \rightarrow O^-(^2P_{3/2}) + O^+(^4S_{3/2}) \quad (4a)$$

$$\rightarrow O_2(R^3\Sigma_u^-) \rightarrow O^-(^2P_{1/2}) + O^+(^4S_{3/2}) \quad (4b)$$

The relative small negative value of β (-0.35) shows that the perpendicular transition is indeed near the resonance peak and the predissociation mechanism (eq 4a) of ion-pair by Rydberg states is able to explain this. In contrast with it, the large positive β (1.64) suggests that, except for the predissociation mechanism (eq 4b), which should have a positive β much smaller than the limiting value 2, a direct dissociation mechanism may be also involved. In fact, in the previously observed O^- photofragment yield spectra, a very weak continuum background exist and they are superimposed on the sharp resonance structure. The continuum background which arises from the direct dissociation will result in a limiting value of $\beta = 2$ for the ion-pair production. Therefore, except the channel of predissociation (eq 4b), the parallel transition may also have the intensities from the continuum absorption. The correlations eqs 4a and 4b should remain the same in this case, however, the Rydberg states are now replaced by the repulsive states with the same symmetry properties. The relative ratios among the predissociation and direct dissociation channels determine the total β we measured. However, a quantitative discussion about β is impossible without detailed theoretical calculations.

It is seen from Table 1 that the branching ratio for producing the low energy component $O^-(^2P_{3/2})$ to the high energy component $O^-(^2P_{1/2})$ is 1:0.78. It is also noted that the energy spacing for the fine structure components[15] is around 177 cm^{-1}, and the available energy for the dissociation is about 10 times larger than this splitting. These facts may illustrate that the dissociation may occur mainly through the adiabatic mechanism. The underlying physics for the mechanism call for detailed calculations on the potential curves of O_2 Rydberg states, ion-pair states and also the fine structure resolved dynamical calculations.

Conclusions

In conclusion, the fine structure resolved photofragment $O^-(^2P_j)$ image from the O_2 ion-pair production at 17.499 eV has been obtained. The experimental results show that the channels for producing the low energy spin−orbit $O^-(^2P_{3/2})$ component and the high energy spin−orbit $O^-(^2P_{1/2})$ component proceed mainly via the intermediate states $O_2(R^3\Pi_u)$ and $O_2(R^3\Sigma_u^-)$, respectively, and the branching ratio for them is 1:0.78. The channel for producing the high energy spin−orbit $O^-(^2P_{1/2})$ component may involve a direct dissociation mechanism.

Acknowledgment. The authors acknowledge the research supports by the National Science Foundation of China under Projects 20273038 and 10274041, the Specialized Research Fund for the Doctoral Program of Higher Education of China, and the NKBRSF of China.

References and Notes

(1) Hatano, Y. *J. Electron Spectrsoc. Relat. Phenom.* **2001**, *119*, 107.
(2) Dehmer, P. M.; Chupka, W. A. *J. Chem. Phys.* **1975**, *62*, 4525.
(3) Berg, L. E.; Erman, P.; Kaellne, E.; Sorensen, S.; Sundstroem, G. *Phys. Scripta.* **1991**, *44*, 328.
(4) Erman, P.; Karawajczyk, A.; Rachlew-Kaellne, E.; Stankiewicz, M.; Franzen, K. Y. *J. Phys. B* **1996**, *29*, 5785.
(5) Ehresmann, A.; Liebel, H.; Schmoranzer, H.; Wilhelmi, O.; Zimmermann, B.; Schartner, K.-H. *J.* Phys. B. **2004**, *37*, 389.

(6) Zare, R. N.; Herschbach, H. R. *Proc. IEEE* **1963**, *51*, 173.
(7) Jonah, C. *J. Chem. Phys*. **1971**, *55*, 1915.
(8) Eppink, A. T. J. B.; Parker, D. H. *Rev. Sci. Instrum*. **1997**, *68*, 3477.
(9) (a) Ahmed, M.; Peterka, D. S.; Regan, P.; Liu, X. H.; Suits, A. G. *Chem. Phys. Lett*. **2001**, *339*, 203. (b) Liu, X. H.; Gross, R. L.; Suits, A. G. *Science* **2001**, *294*, 2527.
(10) Li, W.; Lucchese, R. R.; Doyuran, A.; Wu, Z.; Loos, H.; Hall, G. E.; Suits, A. G. *Phys. Rev. Lett*. **2004**, *92*, 083002.
(11) Yang, J.; Hao, Y.; Li, J.; Zhou, C.; Mo, Y. *J. Chem. Phys*. **2005**, *122*, 134308.
(12) Mo, Y.; Yang, J.; Chen, C. *J. Chem. Phys*. **2004**, *120*, 1263.
(13) Smith, L. M.; Keefer, D. R.; Sudharsanan, S. I. *J. Quant. Spectrosc. Radiat. Transfer* **1988**, *39*, 367.
(14) Gonzalez, R. C.; Woods, R. E. *Digital Image Processing*, 2nd ed.; Prentice Hall: New York, 2002.
(15) Neumark, D. M.; Lykke, K. R.; Andersen, T.; Lineberger, W. C. *Phys. Rev. A* **1985**, *32*, 1890.
(16) Martin, J. D. D.; Hepburn, J. W. *Phys. Rev. Lett*. **1997**, *79*, 3154.
(17) Pratt, S. T.; McCormack, E. F.; Dehmer, J. L.; Dehmer, P. M. *Phys. Rev. Lett*. **1992**, *68*, 584.
(18) Song, Y.; Evans, M.; Ng, C. Y.; Hsu, C. W.; Jarvis, G. K. *J. Chem. Phys*. **1999**, *111*, 1905.
(19) Yoshino, K.; Tanaka, Y. *J. Chem. Phys*. **1968**, *48*, 4859.